Extended Data Fig. 1. Related to Fig. 1.

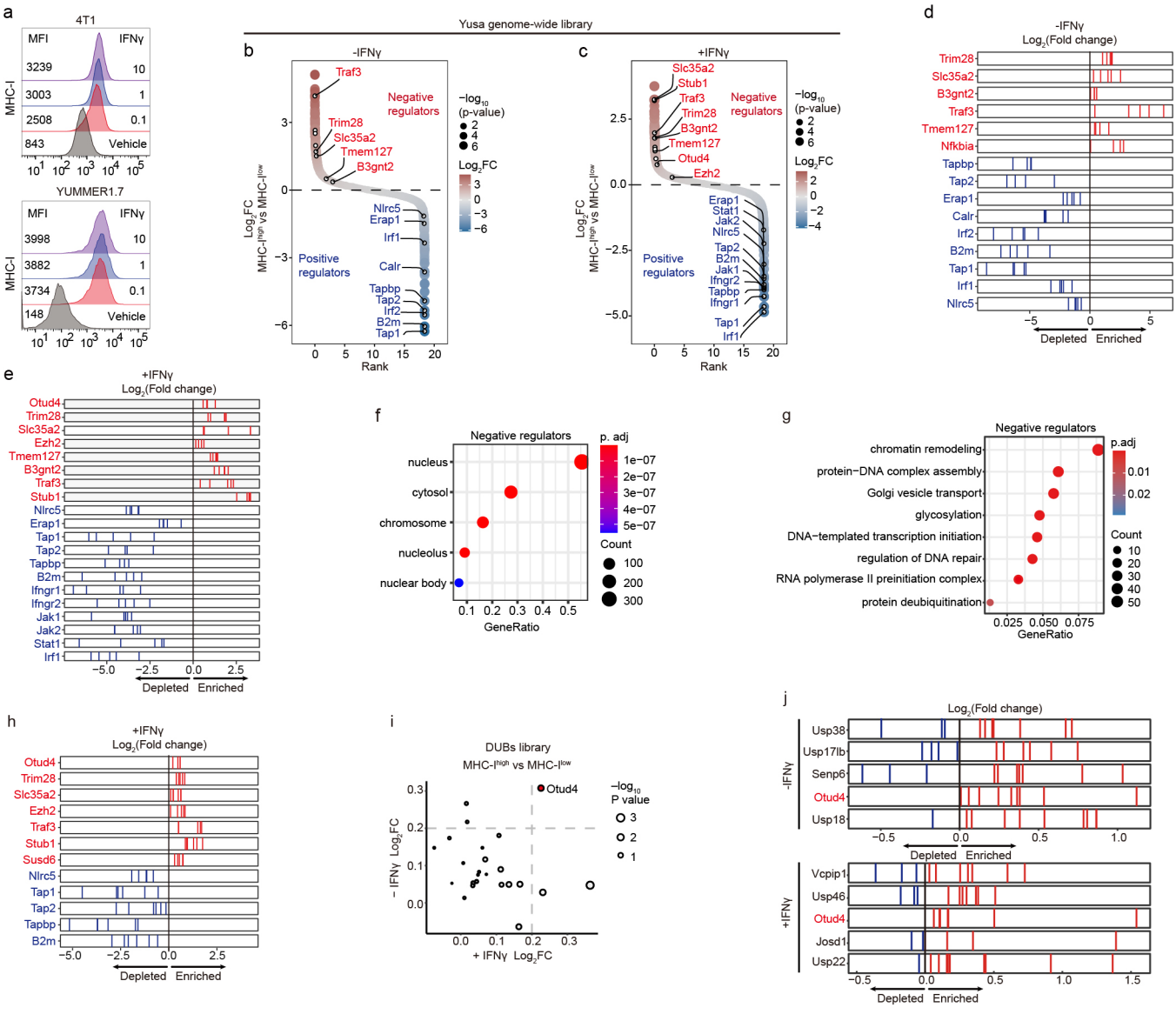

Extended Data Fig. 1. Related to Fig. 1. a. Titration of IFNγ concentration to assess its effect on MHC-I expression. Histograms showing MHC-I levels in 4T1 and YUMMER1.7 cells following a 2-day treatment with varying concentrations of IFNγ, as determined by flow cytometry. b, c. Genome-wide CRISPR screening reveals novel MHC-I regulators in presence (b) or absence (c) of IFNγ. Ranked dot plots depict the enrichment of genes in the MHC-I-high subpopulation compared to the MHC-I-low subpopulation. The X-axis indicates the rank of each gene, while the Y-axis represents the $\log_2$ enrichment of sgRNAs targeting each gene. d, e. Frequency histograms of $\log_2$ fold changes from the genome-wide CRISPR screen in presence (d) or absence (e) of IFNγ. Selected regulators identified in the genome-wide CRISPR screen are shown, highlighting their enrichment patterns. f, g. Functional categories of MHC-I candidate repressors identified through enrichment analysis. h. Frequency histograms of $\log_2$ fold changes from the nucleolomics-related CRISPR screen. i. Deubiquitinase-targeted CRISPR screening identifies novel regulators of MHC-I. Ranked dot plots highlight the enrichment of deubiquitinase-related genes in the MHC-I-high subpopulation compared to the MHC-I-low subpopulation, showing potential regulons. j. Frequency histograms of $\log_2$ fold changes from the deubiquitinase-focused CRISPR screen. Selected regulators identified in the deubiquitinase-targeted screen are displayed.

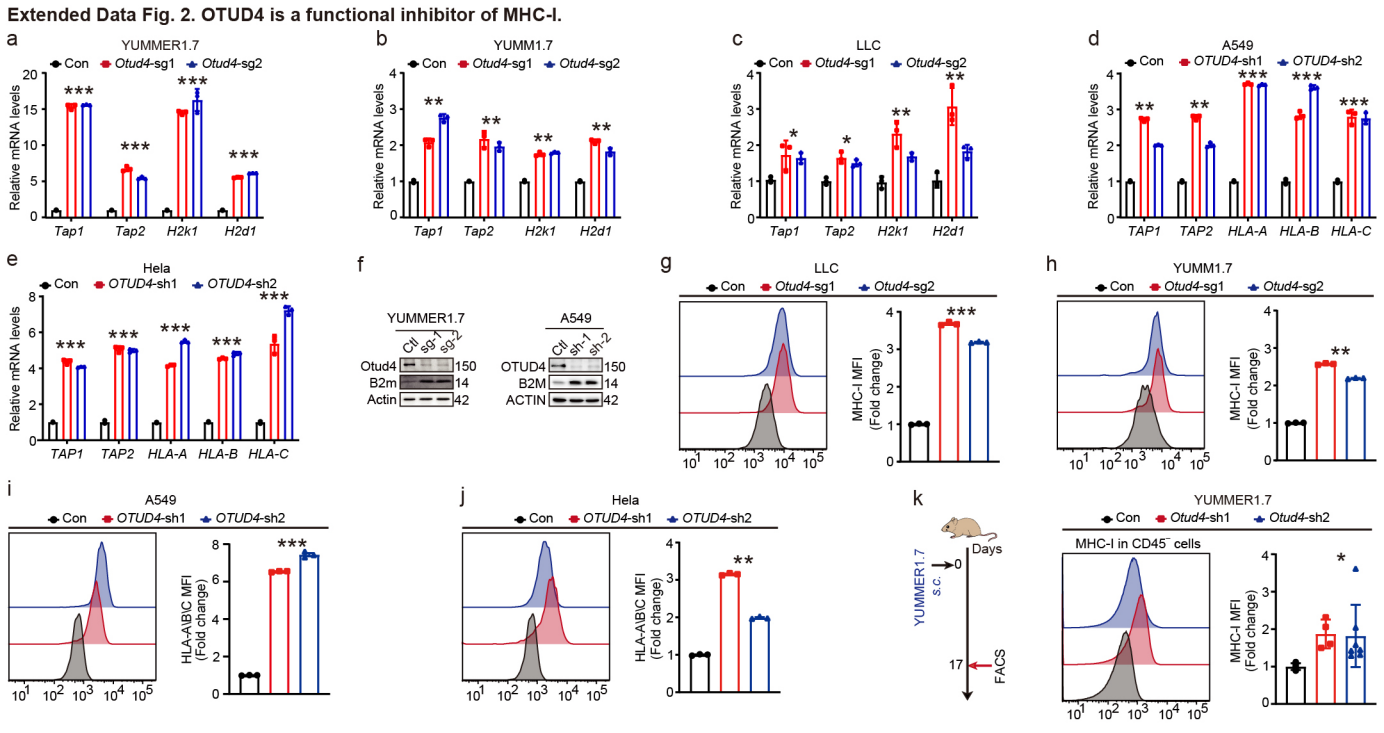

Extended Data Fig. 2. OTUD4 is a functional inhibitor of MHC-I. a-e. Quantitative RT-PCR analysis revealed that *Otud4* deletion upregulated antigen presentation genes, including *Tap1, Tap2, H2-k1,* and *H2-d1*, in murine tumor cell lines (YUMMER1.7, YUMM1.7 and LLC) and human tumor cell lines (A549 and Hela) (n = 3). Data are normalized to the control group. f. Immunoblots of B2M expression. Western blot analysis of B2M expression in control and OTUD4-deficient cells. g-j. Flow cytometry analysis of MHC-I or HLA surface expression. Representative histograms (left) and bar plots (right) depict surface expression of MHC-I in murine tumor cells (LLC and YUMM1.7) and HLA-A/B/C in human tumor cells (A549 and Hela). Quantification of median fluorescence intensity (MFI) is normalized to control sgRNA (Con) groups (n = 3). k. MHC-I surface expression in tumors with *Otud4* knockdown. Surface MHC-I expression was measured in YUMMER1.7 tumors transduced with shRNA targeting *Otud4* or control vectors, harvested 14 days post-transplantation (n ≥ 4). Data represent one experiment. Data are mean ± s.e.m. Statistical significance was determined using two-way ANOVA with Benjamini–Hochberg correction. ns, not significant; *P < 0.05, **P < 0.01 and ***P < 0.001.

Extended Data Fig. 3. OTUD4 deficiency induces adaptive immune-mediated tumor regression across multiple models.

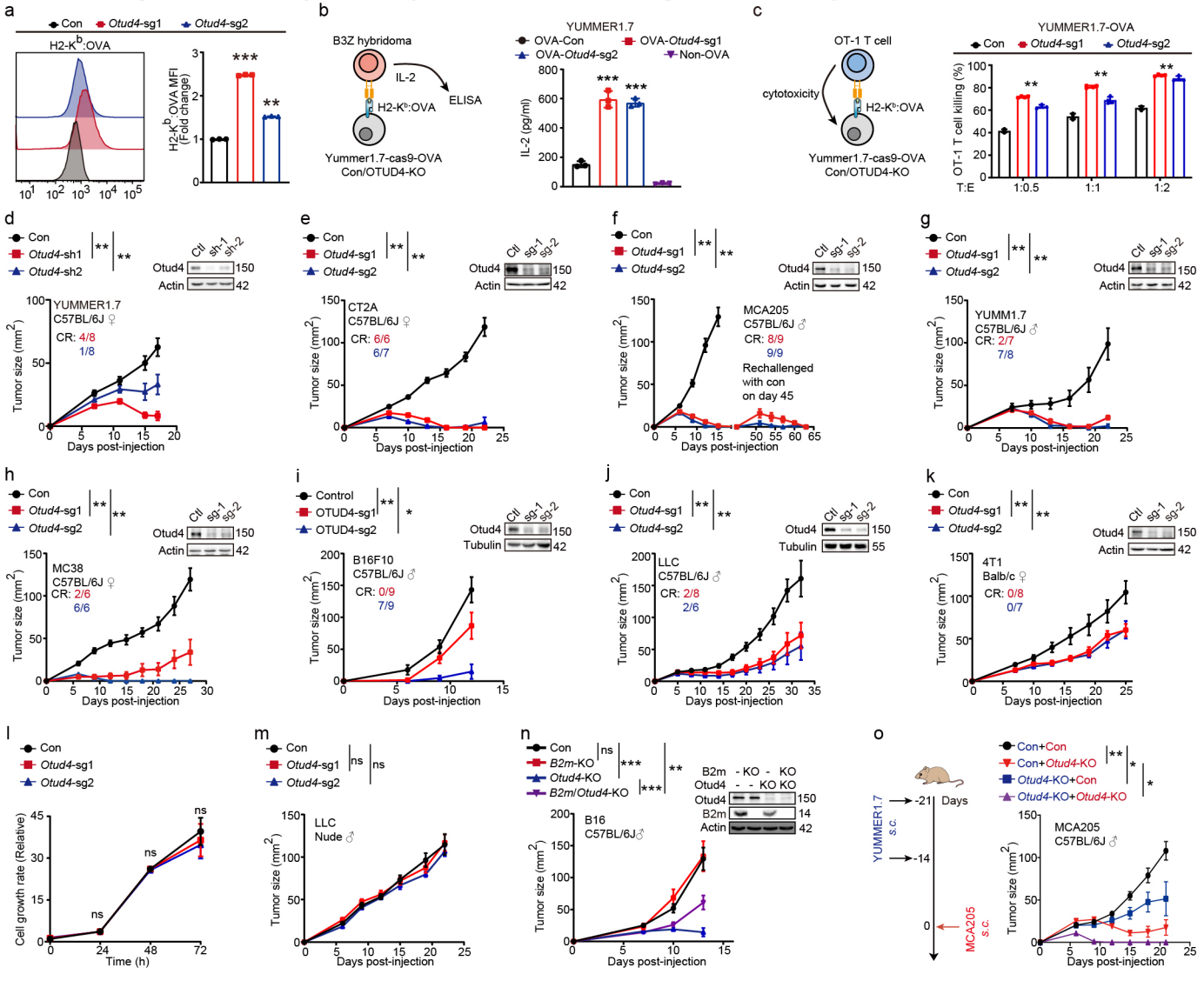

Extended Data Fig. 3. OTUD4 deficiency induces adaptive immune-mediated tumor regression across multiple models. a. Surface expression of H-2Kb: OVA in YUMMER1.7-Cas9-OVA cells. Representative histograms (left) and bar plots (right) show surface expression of H-2Kb: OVA in cells transduced with sgRNAs targeting *Otud4* or controls (n = 3). b. Schematic representation of the T cell activation assay and quantification of IL-2 secretion by B3Z T cell hybridomas co-cultured with YUMMER1.7-Cas9-OVA cells transduced with sgRNAs targeting *Otud4* or controls. (n = 3). c. Schematic of the T cell-mediated cytotoxicity assay and quantification of YUMMER1.7-Cas9-OVA (T) cells killed by OT-1 T cells (E), shown as a bar plot. (n = 4). d-k. Tumour growth in immunocompetent mice transplanted with the indicated tumor cell lines: YUMMER1.7 (d), CT2A (e), MCA205 (f), YUMM1.7 (g), MC38 (h), B16F10 (i), LLC (j), and 4T1 (k) cells transduced with control or *Otud4*-targeting sgRNAs or shRNAs. *Otud4* knockdown or knockout in tumor cells was validated via immunoblotting. (n ≥ 6) l. Proliferation rates of wild-type and *Otud4*$^{-/-}$ YUMMER1.7 cells, as assessed by a CCK8 assay at 24 and 48 hours. Growth rates were normalized to the control sgRNA (Con) group at 0 hours. (n = 3). m. Tumor area quantification in nude mice transplanted with LLC cells transduced with the indicated sgRNAs. (n ≥ 6). n. Tumor area quantification in immunocompetent mice transplanted with B16F10 cells transduced with the indicated sgRNAs (n ≥ 6). B16F10 cells were treated with 10 ng/mL IFNγ for 24 h. After that, knockout of Otud4 and B2m in various tumor cells validated by immunoblotting. o. Tumor growth curves in C57BL/6J mice that initially rejected control or *Otud4*$^{-/-}$ YUMMER1.7 tumors (blue) and were subsequently rechallenged with control or *Otud4*$^{-/-}$ MCA205 cells (red) (n ≥ 7). Data represent one experiment. Data are mean ± s.e.m. Statistical significance was determined using two-way ANOVA with Benjamini–Hochberg correction. *P < 0.05, **P < 0.01 and ***P < 0.001.

Extended Data Fig. 4. Deletion of OTUD4 in cancer cells inflames TIME.

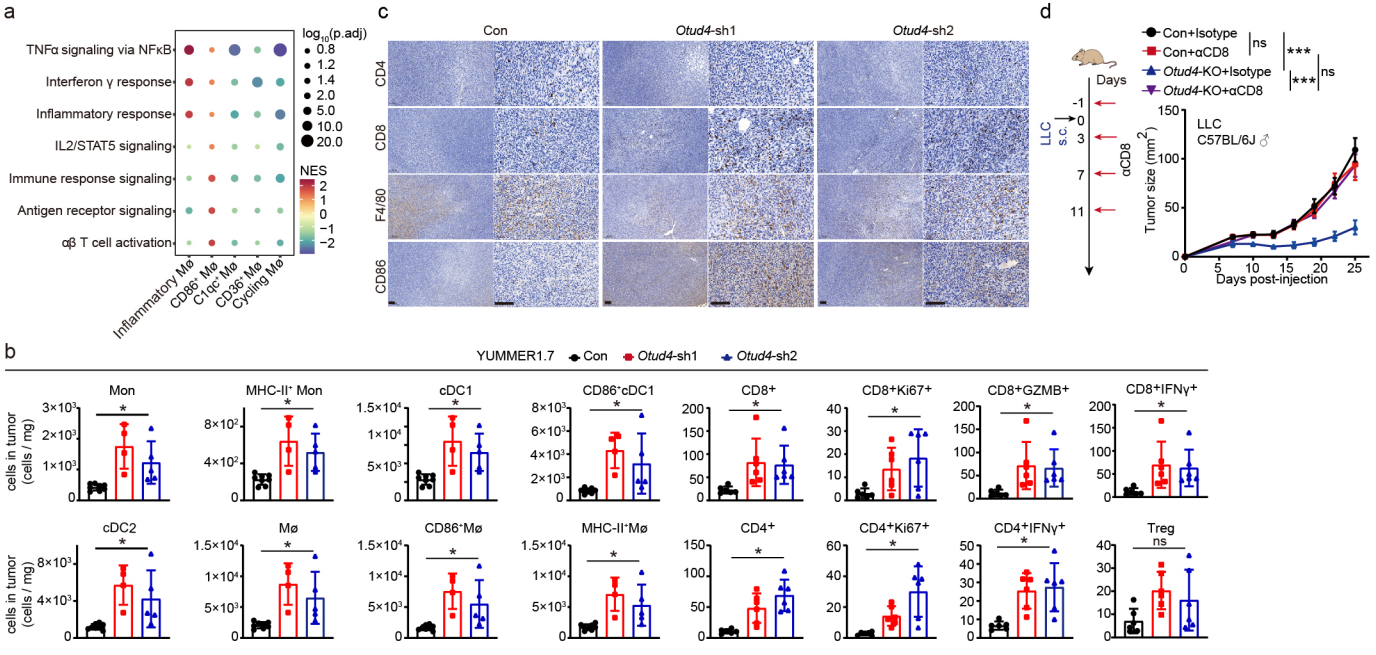

Extended Data Fig. 4. Loss of OTUD4 in tumor cells inflames TIME. a. Pathway enrichment analysis of macrophage subpopulations revealed distinct functional pathways. Marker size reflects the P value, while color intensity represents the normalized enrichment score. b. Flow cytometric analysis comparing immune cell populations in control versus *Otud4*-deficient YUMMER1.7 tumors. c. Representative immunohistochemical staining of CD4 (CD4$^+$ T cells), CD8 (CD8$^+$ T cells), F4/80 (macrophages), and CD86 in control and *Otud4*-deficient YUMMER1.7 tumors 14 days post-injection. Scale bar = 100 μm. d. Tumor growth curves for control and *Otud4*-deficient LLC tumors in mice treated with anti-CD8 antibody. (n = 10). Data represent a single experiment and are presented as mean ± s.e.m. Statistical significance was determined using two-way ANOVA with Benjamini–Hochberg correction. ns, not significant; *P < 0.05, **P < 0.01 and ***P < 0.001.

Extended Data Fig. 5. Related to Fig. 2.

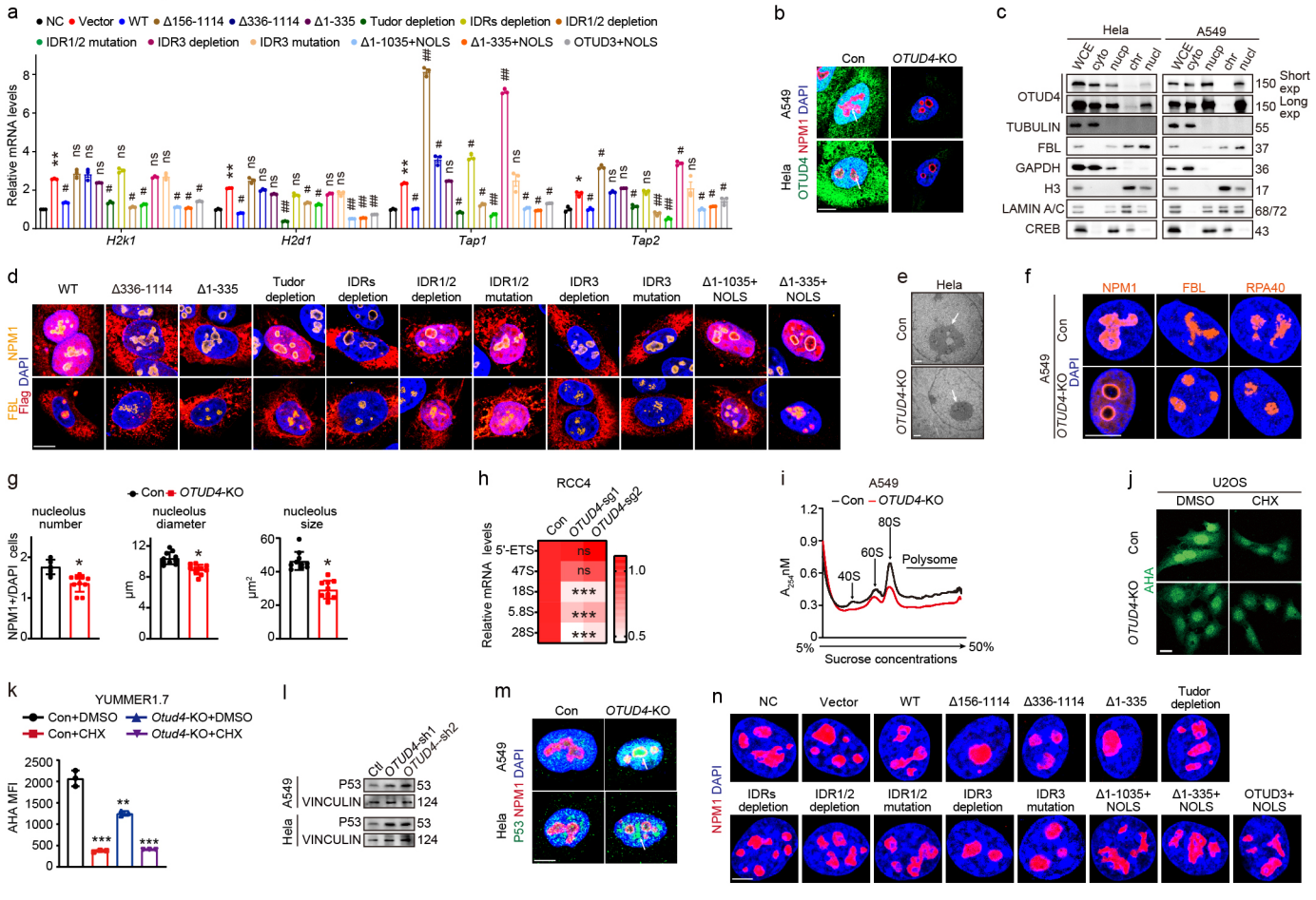

Extended Data Fig. 5. Related to Fig. 2. a. qRT-PCR analysis of MHC-I AP genes in control and *Otud4*$^{-/-}$ YUMMER1.7 cells overexpressing the indicated truncations (n = 3). b. Representative immunofluorescence co-staining of OTUD4 (green) and NPM1 (red) in wild-type and *OTUD4*-ablated A549 and Hela cells. Scale bar = 10 μm. c. Immunoblot analysis of OTUD4 in whole-cell extract (WCE), cytoplasmic (cyto), nucleoplasmic (nucp), chromatin (chr), and nucleolar (nucl) fractions of A549 and Hela cells. d. Representative immunofluorescence staining of wild-type OTUD4 and OTUD4 truncations. Scale bar = 10 μm. e. Transmission electron micrographs showing nuclear and nucleolar morphology in control and *OTUD4*-deficient Hela cells. Nucleoli (white) are marked as indicated. Scale bar = 0.5 μm. f. Immunostaining (left) of nucleolar markers NPM1, FBL, and RPA40 in control and *OTUD4*-deficient A549 cells. Scale bar = 10 μm. g. Quantification (right) of nucleolar number, diameter, and size in the indicated cell lines. Nucleoli were identified by NPM1 staining and manually quantified. Statistical significance was determined using Two-sided Student's t-test. h. qRT-PCR analysis of pre-rRNA expression in control and *OTUD4*$^{-/-}$ RCC4 cells (n = 3). Statistical significance was determined using two-way ANOVA with Benjamini–Hochberg correction. i. Polysome profiling of control and *OTUD4*$^{-/-}$ A549 cells analyzed using sucrose density gradient ultracentrifugation. j. Representative AHA-labeled immunofluorescence staining of sgCon or sg*OTUD4* U2OS cells with or without CHX treatment. Scale bar = 10 μm. k. Bar plots showing quantification of AHA-labeled MFI by flow cytometry in control and *Otud4*$^{-/-}$ YUMMER1.7 cells with or without CHX treatment. Statistical significance was determined using two-way ANOVA with Benjamini–Hochberg correction. l. Western blot analysis of P53 expression in the indicated cell lines. m. Representative immunofluorescence co-staining of P53 (green) and NPM1 (red) in the indicated cell lines. Scale bar = 10 μm. n. Representative immunofluorescence staining of NPM1 (red) in control or *Otud4*$^{-/-}$ YUMMER1.7 cells overexpressing the indicated truncations. Scale bar = 10 μm. Data represent a single experiment and are presented as mean ± s.e.m. ns, not significant; *P < 0.05, **P < 0.01 and ***P < 0.001 compared to the control; #P < 0.05, ##P < 0.01 and ###P < 0.001 compared to the vector group.

Extended Data Fig. 6. OTUD4 catalyses K63-linked deubiquitination of NPM1 to stabilize its oligomerization

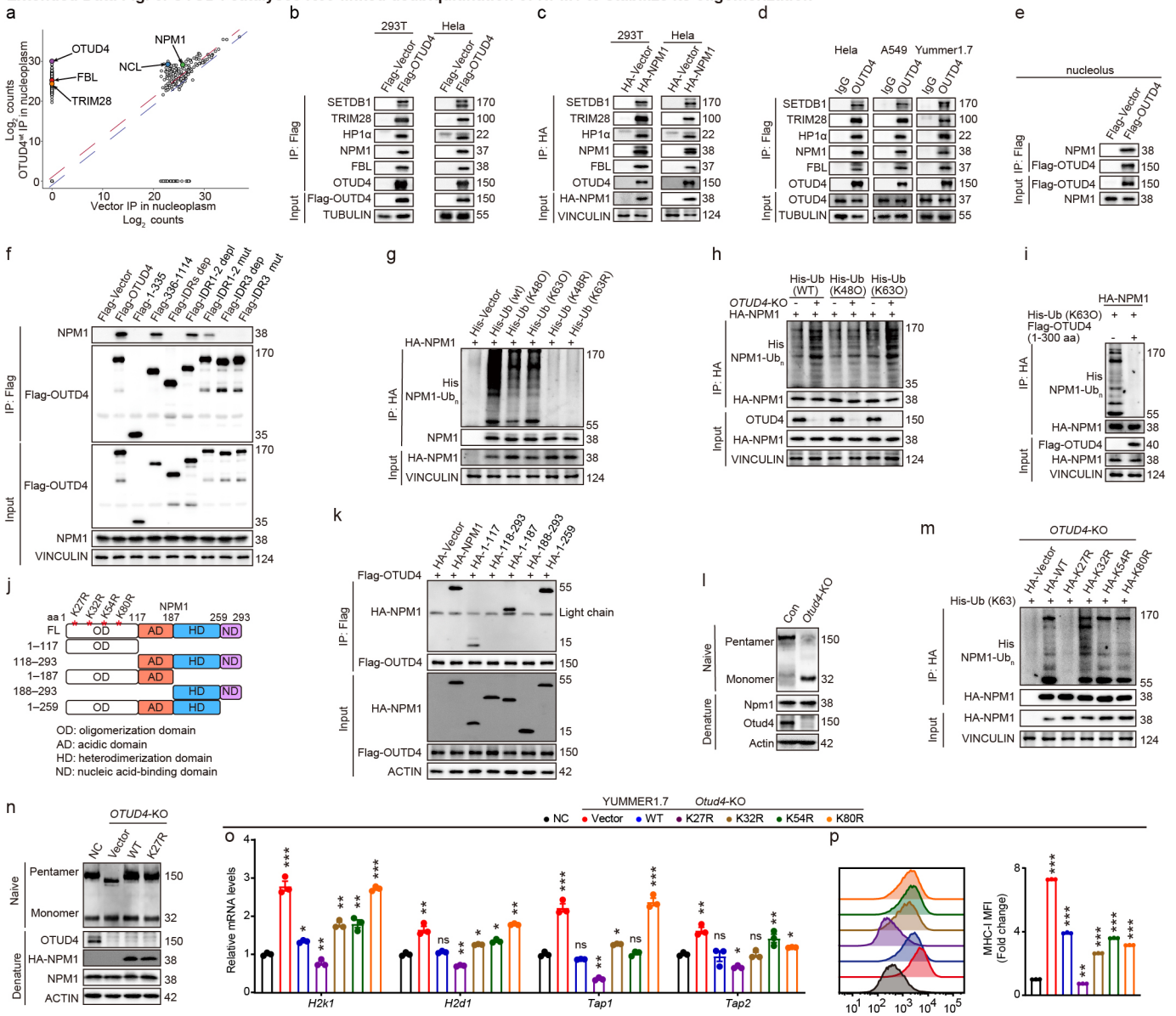

Extended Data Fig. 6. OTUD4 catalyses K63-linked deubiquitination of NPM1 to stabilize its oligomerization. a. IP-mass analysis of OTUD4-binding proteins in the nuclear fraction. Nucleophosmin 1, NPM1; Fibrillarin, FBL; Nucleolin, NCL; Tripartite Motif Containing 28, TRIM28. b-c. Flag or HA immunoprecipitation was performed from HEK293 and Hela cells expressing the indicated vectors and western blotted as shown. d. Endogenous immunoprecipitation performed from Hela, A549, and YUMMER1.7 cells using control IgG and OTUD4 antibody. e. Co-immunoprecipitation of Flag-OTUD4 with HA-NPM1 in nucleolar fractions. f. Flag immunoprecipitation of HEK293 cells transfected with plasmids encoding HA-NPM1 and Flag-tagged OTUD4 WT or truncates. g. HA-NPM1 and His-Ub wild-type or mutants were expressed in HEK293 cells, HA-immunoprecipitated after SDS denaturation, and blotted as indicated. h. HA-NPM1 and His-Ub wild-type were expressed in wild-type or *OTUD4*-deleted HEK293 cells, HA-immunoprecipitated after SDS denaturation, and blotted as shown. i. OTUD4 directly removes K63-linked ubiquitin from NPM1 in vitro. j. Schematic of domain organization of wild-type NPM1 and its various mutants/truncations used in this study. k. Flag Co-immunoprecipitation of HEK293 cells transfected with plasmids encoding Flag-tagged OTUD4 and HA-NPM1 or truncates. l. Image of native PAGE with anti-NPM1 showing oligomeric and monomeric NPM1 proteins in control and *Otud4*-knockout YUMMER1.7 cells \. m. His-Ub (K63O) and HA-NPM1 wild-type or mutants were transfected into *OTUD4*-deleted HEK293 cells, HA-immunoprecipitated after SDS denaturation, and blotted as shown. n. Image of native PAGE with anti-NPM1 showing oligomeric and monomeric NPM1 proteins in control or *Otud4*$^{-/-}$ YUMMER1.7 cells overexpressing empty vector control, wild-type NPM1, or mutants. o. qRT-PCR analysis of MHC-I antigen processing genes in control or *Otud4*$^{-/-}$ YUMMER1.7 cells overexpressing empty vector control, wild-type NPM1, or mutants as indicated (n = 3). p. Typical histograms (left) and bar plots (right) of MHC-I flow cytometry in control or *Otud4*$^{-/-}$ YUMMER1.7 cells overexpressing empty vector control, wild-type NPM1, or mutants as indicated (n = 3). MFI quantification is normalized to the Con group. For gel source data, see Supplementary Fig. 2. Data represent a single experiment and are presented as mean ± s.e.m. Statistical significance was determined using two-way ANOVA with Benjamini–Hochberg correction. ns, not significant; *P < 0.05, **P < 0.01 and ***P < 0.001 compared to the control; #P < 0.05, ##P < 0.01 and ###P < 0.001 compared to the vector group.

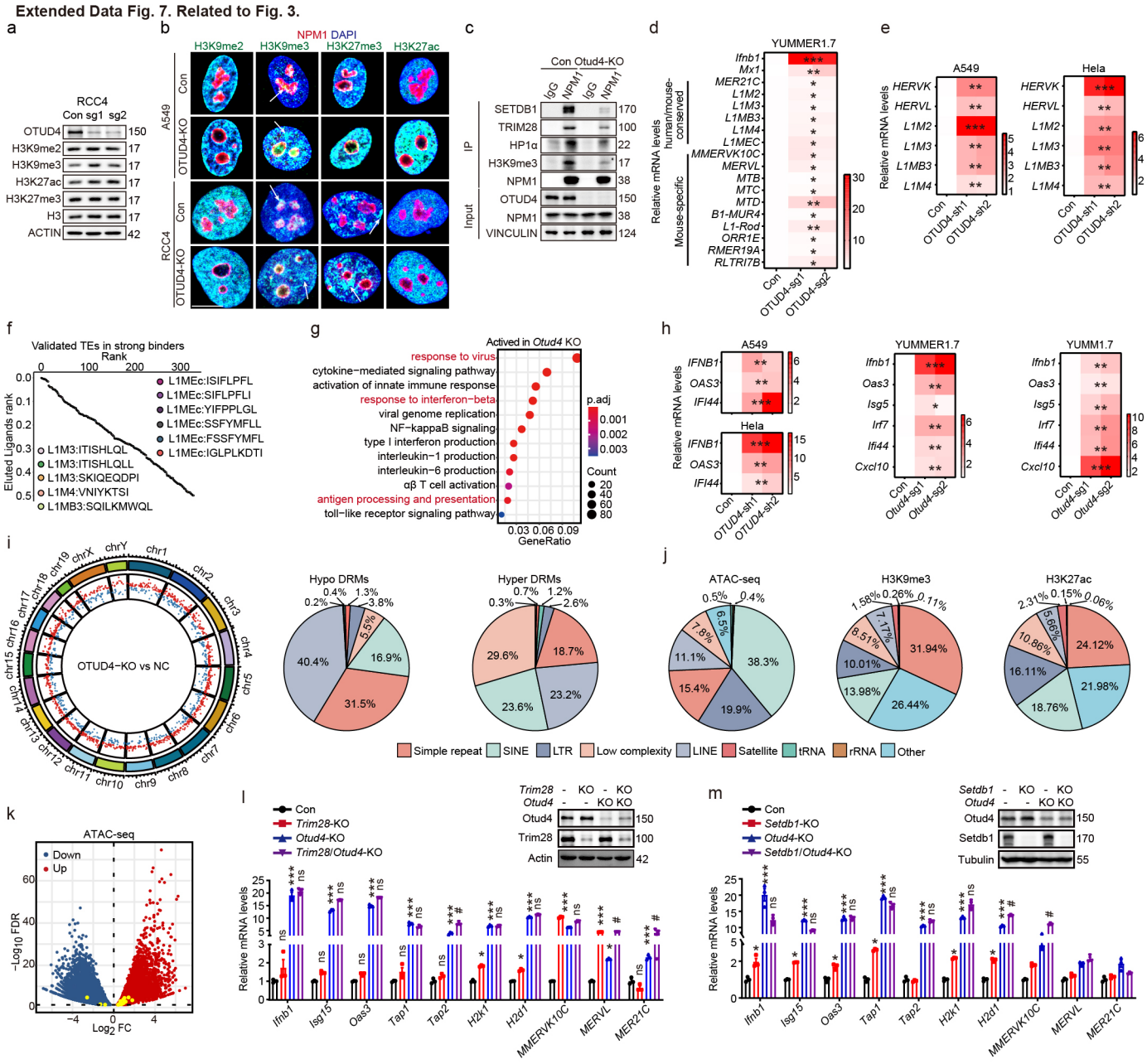

Extended Data Fig. 7. Related to Figure 3. a. Immunoblots of the indicated chromatin modifications in control or *OTUD4*$^{-/-}$ RCC4 cells. b. Representative immunofluorescence co-staining of chromatin modifications including H3K9me2, H3K9me3, H3K27me3, H3K27ac (green) and NPM1 (red) in wild-type or *OTUD4*-ablated A549 and RCC4 cells. Scale bar = 10 μm. c. Endogenous immunoprecipitation performed using control IgG and NPM1 antibody in control or *Otud4*$^{-/-}$ YUMMER1.7 cells. d. RT-qPCR analyses of the indicated ERVs in control and *Otud4*$^{-/-}$ YUMMER1.7 cells (n=3). Statistical significance was determined using two-way ANOVA with Benjamini–Hochberg correction. e. RT-qPCR analyses of the indicated ERVs in control and *OTUD4*$^{-/-}$ A549 and Hela cells (n=3). f. Rank diagram depicting predicted unique H2-Kb/H2-Db-binding peptides encoded by ERVs in *Otud4*$^{-/-}$ versus control YUMMER1.7 cells based on RNA-seq analysis. g. Pathway enrichment map of upregulated domains in *Otud4*$^{-/-}$ versus control YUMMER1.7 cells, derived from Gene Ontology (GO) analyses of ATAC-seq data. h. RT-qPCR analysis of interferon-stimulated genes (ISGs) in control and *OTUD4*$^{-/-}$ A549, Hela, YUMM1.7, and YUMMER1.7 cells (n = 3). i. Cycle diagrams deciphering the distribution of methylation sites (left) and ERV annotations (right) in whole-genome bisulfite sequencing (WGBS). j. ERVs annotation in transposase-accessible chromatin with high-throughput sequencing (ATAC-seq) peaks or H3K9me3- or H3K27ac-binding peaks in YUMMER1.7 cells (n=2). k. Volcano plot highlighting retroelement loci with significantly increased (red) or decreased (blue) expression (FDR-adjusted P < 0.05) in *Otud4*$^{-/-}$ versus control YUMMER1.7 cells, based on ATAC-seq data. The yellow dots denote L1MEc retroelements. l. RT-qPCR analysis of ISG genes, MHC-I AP genes, and ERVs in control and *Otud4*$^{-/-}$ YUMMER1.7 cells with or without *Trim28* depletion (n = 3). m. RT-qPCR analysis of ISG genes, MHC-I AP genes, and ERVs in control and *Otud4*$^{-/-}$ YUMMER1.7 cells with or without *Setdb1* depletion (n = 3).Data represent a single experiment and are presented as mean ± s.e.m. Statistical significance was determined using two-way ANOVA with Benjamini–Hochberg correction. ns, not significant; *P < 0.05, **P < 0.01 and ***P < 0.001 compared to the control; #P < 0.05, ##P < 0.01 and ###P < 0.001 compared to the vector or OTUD4-ablated group.

Extended Data Fig. 8. Retroelements activated by OTUD4 deletion stimulate type-I interferon and MHC-I antigen presentation through DNA-sensing pathways

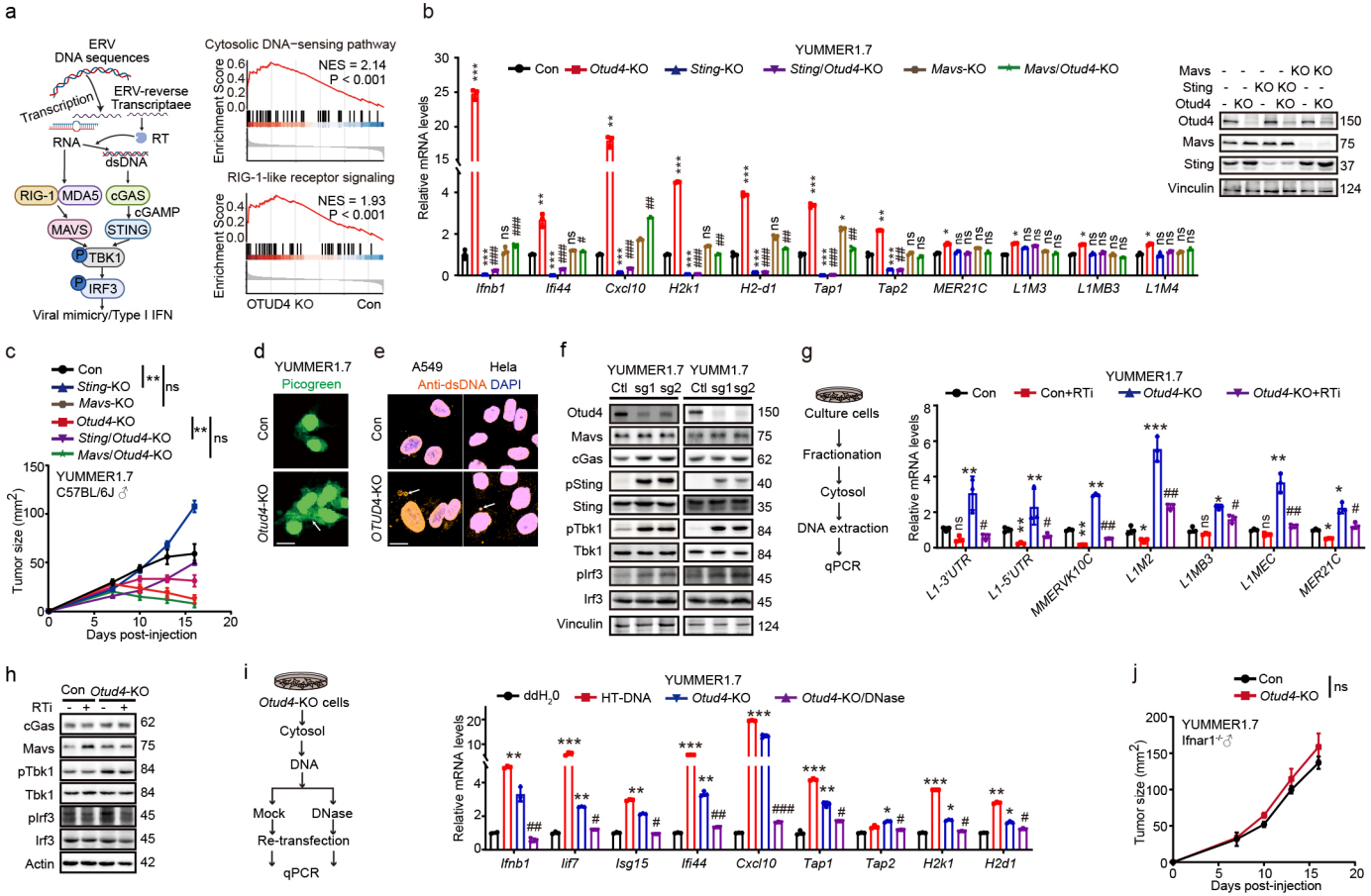

Extended Data Fig. 8. Retroelements activated by OTUD4 deletion stimulate type-I interferon and MHC-I antigen presentation through DNA-sensing pathways. a. Schematic illustrating the process of retroelement activation and nucleic acid-sensing pattern recognition receptor signaling. Gene set enrichment analysis of two top pathways induced by *Otud4* deletion in YUMMER1.7 cells. FDR, false discovery rate; NES, normalized enrichment score. b. RT-qPCR analyses of the indicated ISGs, MHC-I AP genes, and ERVs in control and *Otud4*$^{-/-}$ YUMMER1.7 cells with or without *Sting* or *Mavs* depletion. Knockout of *Otud4, Sting,* and *Mavs* in various tumor cells validated by immunoblotting. c. Immunocompetent C57BL/6J mice were injected subcutaneously with the indicated cells. Tumor growth curves of these cells were analyzed (n ≥ 8). d. Control or *Otud4*-KO YUMMER1.7 cells were stained with 1 mL/mL PicoGreen (green). Scale bar = 10 μm. e. Immunofluorescence staining of control or *OTUD4*-KO A549 (right) and Hela (left) cells with anti-dsDNA antibody. Scale bar = 10 μm. f. Western blot analyses of MAVS and DNA sensing signaling proteins. T-, total; p-, phosphorylated. For gel source data, see Supplementary Fig. 2. g-h. Workflow (left) and RT–qPCR analyses (right) of the indicated ERVs (g) in control or *Otud4*$^{-/-}$ YUMMER1.7 cells treated with or without a reverse transcriptase inhibitor (RTi, 10 μM) for 48 h. Each ERV level in cytosolic DNA was normalized to its expression in DNA isolated from nuclear lysate and the control group. Western blot analyses of DNA sensing signaling proteins (h) . T-, total; p-, phosphorylated. For gel source data, see Supplementary Fig. 2. i. Workflow (left) and RT–qPCR analyses (right) of ISGs and MHC-I AP genes in YUMMER1.7 cells transfected with cytosolic dsDNA. j. Tumor growth curves of control or *Otud4*$^{-/-}$ YUMMER1.7 cells in *Ifnar1*$^{-/-}$ mice. (n = 5). Data represent a single experiment and are presented as mean ± s.e.m. Statistical significance was determined using two-way ANOVA with Benjamini–Hochberg correction. ns, not significant; *P < 0.05, **P < 0.01 and ***P < 0.001 compared to the control; #P < 0.05, ##P < 0.01 and ###P < 0.001 compared to the OTUD4-ablated group.

Extended Data Fig. 9. Phosphorylation of OTUD4 controls its activity.

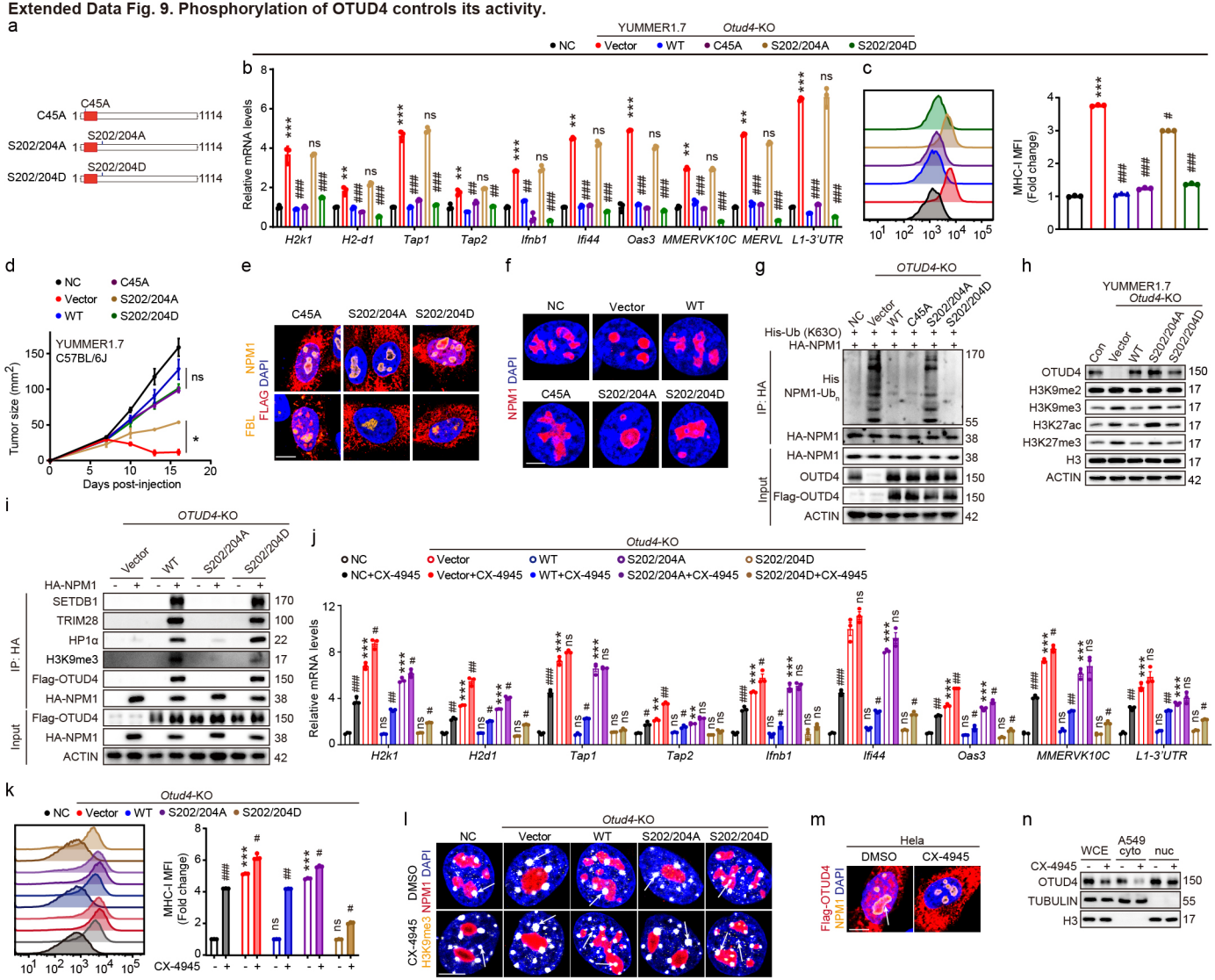

Extended Data Fig. 9. Phosphorylation of OTUD4 controls its activity. a. Schematic illustration of the mutations in OTUD4 used in this study. b. qRT-PCR analysis of MHC-I AP genes in control and *Otud4*$^{-/-}$ YUMMER1.7 cells overexpressing the indicated mutations (n = 3). c. Representative histograms (left) and bar plots (right) from flow cytometry analysis of MHC-I surface expression in control and *Otud4*$^{-/-}$ YUMMER1.7 cells overexpressing the indicated mutations. Median fluorescence intensity (MFI) values are normalized to the control (Con) group (n = 3). d. Tumor growth curves of control and *Otud4*$^{-/-}$ YUMMER1.7 cells overexpressing the indicated mutations in mice (n = 10). e. Representative immunofluorescence staining of OTUD4 mutations. Scale bar = 10 μm. f. Representative immunofluorescence staining of NPM1 (red) in control or *Otud4*$^{-/-}$ YUMMER1.7 cells overexpressing the indicated mutations. Scale bar = 10 μm. g. HA-NPM1 and His-Ub (K63O) as well as empty vector control, wild-type OTUD4, or OTUD4 mutants were expressed in *OTUD4*$^{-/-}$ HEK293 cells, HA-immunoprecipitated after SDS denaturation, and blotted as shown. h. Immunoblots of the indicated chromatin modifications in control or *Otud4*$^{-/-}$ YUMMER1.7 cells overexpressing vector control, wild-type OTUD4, or OTUD4 mutants. i. HA-tagged co-immunoprecipitation of *OTUD4*$^{-/-}$ HEK293 cells transfected empty vector control, wild-type OTUD4, or OTUD4 mutants as well as HA-NPM1 plasmids. HA-immunoprecipitated after SDS denaturation, and blotted as shown. j-l. Control or Otud4$^{-/-}$ YUMMER1.7 cells overexpressing empty vector control, wild-type OTUD4 or OTUD4 or mutants as indicated, and then treated with or without CX-4945 (10 μM) for 24 h. RT–qPCR analyses of ISGs, MHC-I AP genes and ERVs were performed (j). flow cytometry analyses of MHC-I were shown (k). Representative immunofluorescence co-staining of chromatin modifications including H3K9me3 (orange) and NPM1 (red) was shown (l). m. Immunofluorescence staining of Flag (orange) and NPM1 (red) in Hela cells transfected with Flag-tagged full-length OTUD4 and treated with or without CX-4945 (20 μM) for 24 h. Scale bar = 10 μm. n. Western blot analyses of OTUD4 in cytoplasmic (cyto) and nucleus (nuc) fractions of YUMMER1.7 treated with or without CX-4945 (10 μM) for 24 h. For gel source data, see Supplementary Fig. 2. Data represent a single experiment and are presented as mean ± s.e.m. Statistical significance was determined using two-way ANOVA with Benjamini–Hochberg correction. ns, not significant; *P < 0.05, **P < 0.01 and ***P < 0.001 compared to the control; #P < 0.05, ##P < 0.01 and ###P < 0.001 compared to the vector group.

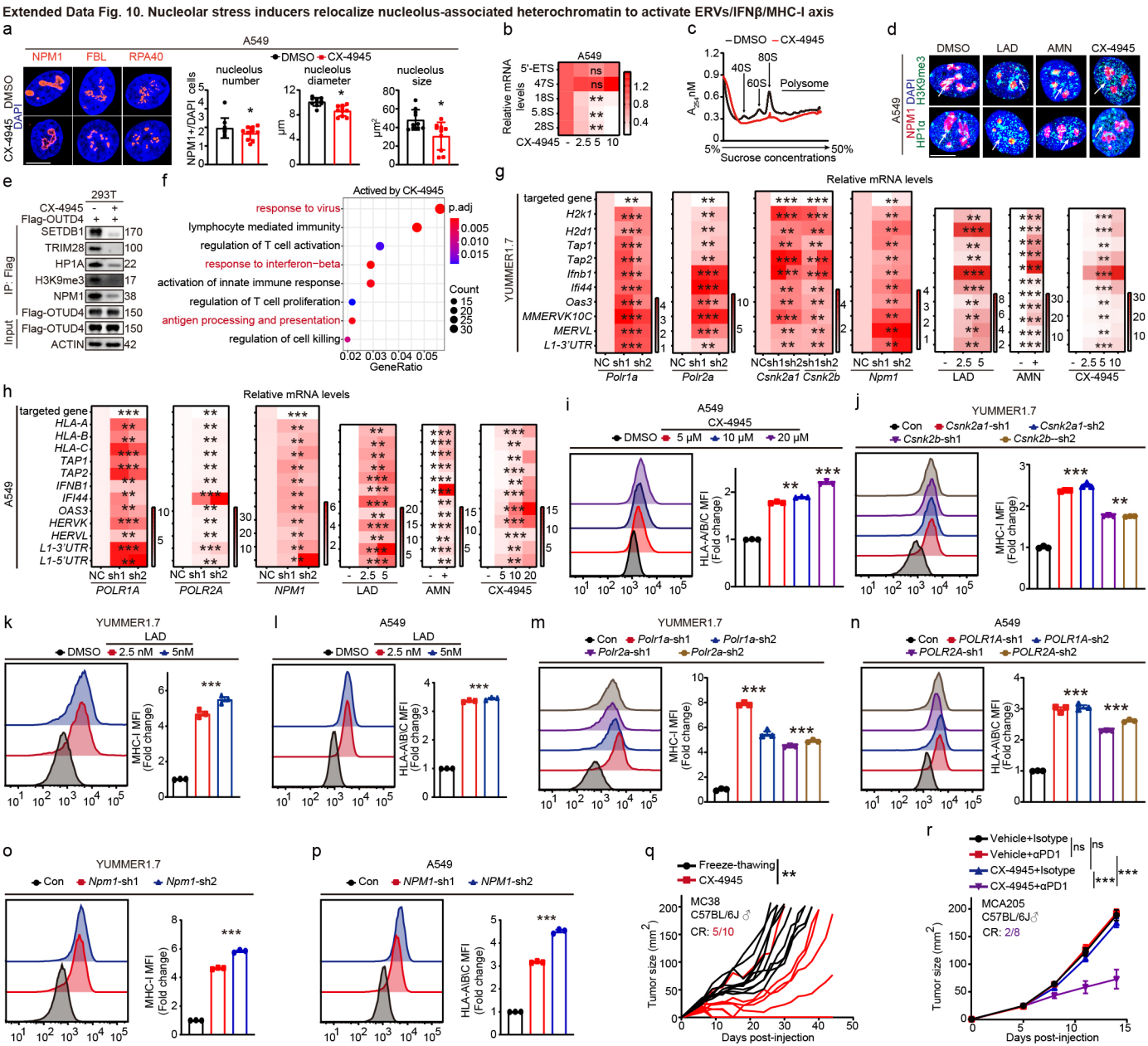

Extended Data Fig. 10. Nucleolar stress inducers relocalize nucleolus-associated heterochromatin to activate ERVs/IFNβ/MHC-I axis. a. Immunostaining of the nucleolus marker NPM1, FBL, and RPA40 in A549 cells treated with or without CX-4945 (20 μM) for 24 h (left). Scale bar = 10 μm. The quantification of nucleolus number, nucleolar diameter, and size in the indicated cell lines (right). The nucleoli were labeled by NPM1 and calculated manually. b. qRT-PCR analysis of pre-rRNA expression in A549 cells treated with or without CX-4945 (20 μM) for 24 h. c. Polysome profiling in A549 cells treated with or without CX-4945 (20 μM) for 24 hours, analyzed using sucrose density gradient ultracentrifugation. d. Representative immunofluorescence co-staining of chromatin modifications including H3K9me3, HP1α (green) and NPM1 (red) in A549 cells with or without actinomycin D (LAD, 5 nM) for 1 h, α-amanitin (AMN, 50 ng/ml) for 16 h, and CX-4945 (20 μM) for 24 h. Scale bar = 10 μm. e. Flag-tagged CoIP of HEK293 cells overexpressing Flag-tagged OTUD4 full length, and then treated with or without CX-4945 (10 μM) for 24 h. Flag-immunoprecipitated after SDS denaturation, and blotted as shown. f. Gene set enrichment analysis of top pathways in YUMMER1.7 cells treated with or without CX-4945. The marker size represents the P value and the color intensity indicates the normalized enrichment score. g-s. YUMMER1.7 or A549 cells were knockdowned with *POLR1A, POLR2A,* CK2 complex (*CSNK2A1* or *CSNK2B*) or *NPM1*. The indicated cells were treated with or without LAD, AMN or CX-4945 as described concentrations for 24 h. RT–qPCR analyses of ISGs, MHC-I AP genes and ERVs were deciphered (g-h). Typical histograms (left) and bar plots (right) of MHC-I or HLA-A/B/C detected by flow cytometry in the indicated cells (i-s). MFI quantification is normalized to the Con group. q. CX-4945-mediated vaccination assay in MC38 tumors. Control mice were injected with necrotic cells induced by five freeze-thaw cycles. (n = 8) r. Tumor growth curves in C57BL/6 mice implanted with MCA205 cells treated with CX4945 alone or in combination with anti-PD-1 antibody were plotted (n ≥ 8). Complete response (CR) was defined as the number of mice achieving a complete response relative to the total number of mice. Data represent a single experiment and are presented as mean ± s.e.m. Statistical significance was determined using two-way ANOVA with Benjamini–Hochberg correction. ns, not significant; *P < 0.05, **P < 0.01 and ***P < 0.001.

Extended Data Fig. 11. OTUD4 is positively correlated with tumor progression and poor prognosis in clinical sample.

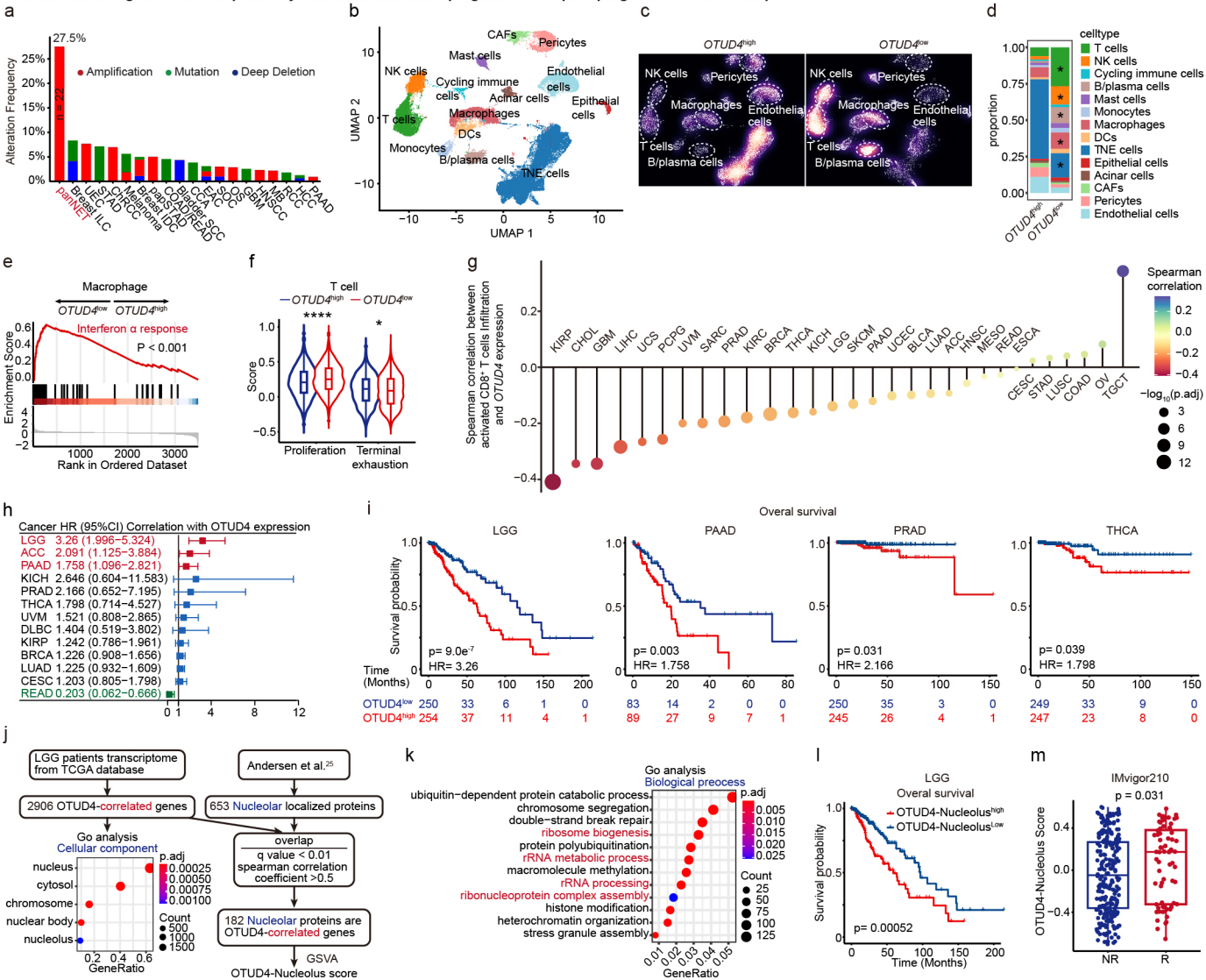

Extended Data Fig. 11. OTUD4 is positively correlated with tumor progression and poor prognosis in clinical sample. a. Distribution and types of *OTUD4* mutations identified from cBioPortal across various cancer types. Cancer types: panNET, pancreatic neuroendocrine carcinoma; ILC, invasive lobular carcinoma; UEC, uterine endometrioid carcinoma; STAD, stomach adenocarcinoma; ChRCC, chromophobe renal cell carcinoma; IDC, invasive ductal carcinoma; papSTAD, papillary stomach adenocarcinoma; COAD, colon adenocarcinoma; READ, rectum adenocarcinoma; SCC, squamous cell carcinoma; CCA, cholangiocarcinoma; EAC, esophageal adenocarcinoma; SOC, serous ovarian cancer; OS, osteosarcoma; GBM, glioblastoma multiforme; HNSCC, head and neck squamous cell carcinoma; MB, medulloblastoma; RCC, renal clear cell carcinoma; HCC, hepatocellular carcinoma; PAAD, pancreatic adenocarcinoma. b. UMAP analysis of all cells (n =56,628) identifying 14 distinct populations based on scRNA-seq from panNET patient samples. c. Condition-specific cell density projections (left) and relative abundances of cell clusters (right). CAFs, cancer-associated fibroblasts. d. Relative abundances of immune cell clusters. e. Mountain plots showing enrichment scores for the interferon-α response gene set in the macrophage cluster. f. Violin plots illustrating representative proliferation and terminal exhaustion signatures in T cell populations. g. Pearson's correlation between *OTUD4* expression and activated CD8+ T cells infiltration (derived from the TISIDB dataset) in TCGA cohorts. Circle size indicates statistical significance (−log10(adjusted P value)) of the Pearson's correlation. Blue and red indicate positive and negative values, respectively. Cancer types: KIRP, kidney renal papillary cell carcinoma; CHOL, cholangiocarcinoma; LIHC, liver hepatocellular carcinoma; UCS, uterine carcinosarcoma; PCPG, pheochromocytoma and paraganglioma; UVM, uveal melanoma; SARC, sarcoma; PRAD, prostate adenocarcinoma; KIRC, kidney renal clear cell carcinoma; BRCA, breast invasive carcinoma; THCA, thyroid carcinoma; KICH, kidney chromophobe; LGG, brain lower-grade glioma; SKCM, skin cutaneous melanoma; UCEC, uterine corpus endometrial carcinoma; BLCA, bladder urothelial carcinoma; LUAD, lung adenocarcinoma; ACC, adrenocortical carcinoma; MESO, mesothelioma; ESCA, esophageal carcinoma; CESC, cervical squamous cell carcinoma, and endocervical adenocarcinoma; LUSC, lung squamous cell carcinoma; OV, ovarian serous cystadenocarcinoma; TGCT, testicular germ cell tumors. h. Hazard ratios (HR) associated with *OTUD4* expression across TCGA datasets. DLBC, lymphoid neoplasm diffuse large B-cell lymphoma. i. Kaplan–Meier survival curves for patients with LGG or PAAD, stratified by OTUD4 expression levels. HR associated with *OTUD4* expression are listed; P values were calculated by log-rank test. j. Two-dimensional transcriptomic screening of the *OTUD4* network revealed associations with nucleolar-localizing proteins in LGG. Cellular components of *OTUD4*-associated genes were identified using Gene Ontology (GO) analysis (bottom). The *OTUD4*-Nucleolus score was calculated using GSVA based on the 182 nucleolar proteins correlated with *OTUD4* mRNA expression in the LGG patient transcriptome. k. Pathway enrichment map for *OTUD4*-associated genes in LGG derived from GO analyses. l. Kaplan–Meier curves showing the association between high or low *OTUD4*-Nucleolus scores and overall survival in LGG patients from the TCGA database. P values were calculated by log-rank test. m. Box plot illustrating *OTUD4*-Nucleolus score expression in non-responders and responders to anti-PD-1 treatment in the IMvigor210 dataset. Statistical significance was determined using Two-sided Student's t-test.

Extended Data Fig. 12. Detailed model of OTUD4-dependent nucleolar homeostasis mediating immunogenicity.

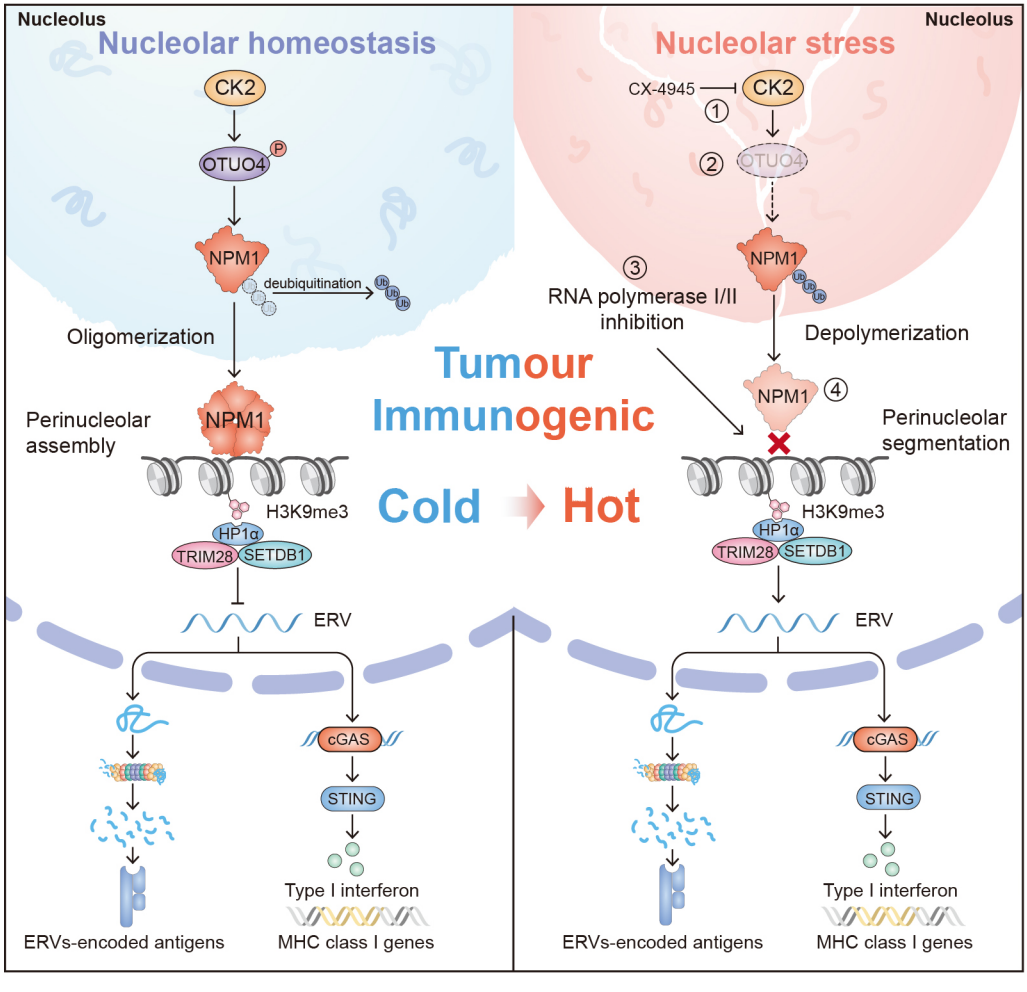

Extended Data Fig. 12. Detailed model of nucleolar OTUD4-dependent nucleolar homeostasis mediating immunogenicity. This model delineates how OTUD4-dependent NPM1 oligomerization governs retroelement-mediated immunogenicity by modulating the spatial distribution of heterochromatin. Within the nucleolus, OTUD4 interacts with NPM1, removing K63-linked ubiquitin chains to facilitate its oligomeric assembly. This process stabilizes the binding betwen NPM1 and H3K9me3-marked heterochromatin. Conversely, OTUD4 depletion disrupts NPM1 oligomerization to induce nucleolar stress and disengage perinucleolar H3K9me3. This heterochromatin disengagement depresses endogenous retroviruses (ERV), resulting in the production of ERV-derived antigens and the upregulation of interferon and MHC-I antigen processing genes via DNA sensor signaling pathways, thereby augmenting tumor immunogenicity. CK2 phosphorylates OTUD4 at the S202/204 sites to specially activate its K63-linked deubiquitinating activity. Inhibition of CK2 with CX-4945 mimics the effect of OTUD4 deficiency, thereby enhancing MHC-I-mediated immunogenicity and potentiating the efficacy of ICB to impede tumor growth. Notably, CK2 inhibitor (①), OTUD4 depletion (②), inhibition of RNA polymerase I or II (③) and NPM1 deficiency (④) converge to instigate nucleolar stress with release of nucleolus-associated heterochromatin H3K9me3 for immunogenicity augmentation.